Received: 21 November 2019 | Revised: 9 January 2020 | Accepted: 15 January 2020

DOI: 10.1002/cjce.23764

THE CANADIAN JOURNAL OF CHEMICAL ENGINEERING

Canadian Society for Chemical Engineering | For Our Future
Société canadienne de génie chimique | Pour notre avenir

ARTICLE

Adding active particles for overall aggregation in a mixing tank: A computational study

Jee Wen Lim | **Jos J. Derksen**

School of Engineering, University of Aberdeen, Aberdeen, UK

Correspondence
Jos J. Derksen, School of Engineering, University of Aberdeen, Aberdeen, UK.
Email: jderksen@abdn.ac.uk

Abstract

In order to achieve flocculation in a dense agitated solid-liquid suspension of nonaggregating particles, we explore scenarios where we add a limited amount of aggregative (ie, active) particles that can bind the nonaggregative particles. The performance of this process hinges on the competition between mixing (spreading the active particles over the flow volume) and aggregation among the active particles, with the latter reducing their effectiveness. The research has been conducted in a computational manner: direct simulations of transitional flow in a mixing tank (at an impeller-based Reynolds number of 4000) are two-way coupled with the dynamics of a collection of spherical, equally sized particles that are given specific aggregative properties. The overall solids volume fraction is 10%. A small fraction of all solid particles (5.8%) is active. Aggregation is quantified by means of the average coordination number as well as the aggregate size distribution. The way the active particles are released in the tank volume has a significant effect on the overall levels of aggregation, specifically for active particles with a strong aggregative force.

KEYWORDS

aggregation, Eulerian-Lagrangian simulation, lattice-Boltzmann method, solid-liquid mixing

1 | INTRODUCTION

Many natural and engineered systems involve mixtures of liquid and fine solid particles. Sediment transport in rivers is an example from the natural environment; the production of high-purity pharmaceutical powders from a supersaturated solution is an example from industry. Understanding and predicting the dynamics of solid-liquid suspensions therefore has relevance in a wide range of applications. The aspect we are focusing on in this paper is aggregation of particles. In many solids-liquid suspensions, particles have a tendency to stick together and form aggregates. There is a variety of reasons for particles to stick to other particles. Physical reasons include van der Waals interactions. Some types of particles have long-chain molecules at their surface that have a tendency to entangle thereby forming aggregates.[1] In crystallization processes, supersaturation in between closely spaced crystals can cause the formation of a solid bridge between them.[2] Aggregation processes are intimately connected to the (fluid) dynamics of solid-liquid suspensions. In order for particles to aggregate they first need to collide. For non-colloidal particles, as will be the subject of this paper, relative motion between particles brought about by fluid flow is the major source of collisions.[3] At the same time, fluid flow and fluid deformation, and its associated stresses, provide mechanisms to disrupt aggregates.[4,5]

There are various approaches to model aggregation. Seminal work was done by Von Smoluchowski.[6] It highlights the role of shear in irreversible aggregation of particles. The Von Smoluchowski equation has been modified

to include several other parameters, for instance the role of shear has been generalized to turbulent flow by relating effective shear to the energy dissipation rate.[7] The population balance equation (PBE) is an important way to model and keep track of size distributions.[8–11]

From an applications point of view, aggregation is a major influencer of the particle size distribution. Product quality and processability are directly linked to the particle size distribution. Aggregation is a desired phenomenon if one wants to quickly grow particles in order to separate them more easily from the liquid phase. The usual way of inducing aggregation is by adding a flocculant, a chemical agent that promotes aggregation by, for instance, shrinking the electrical double layers of particles thereby suppressing electrostatic repulsion.[12] In this paper we follow an alternative route to aggregation and are interested in promoting aggregation of an initially nonaggregative system by adding aggregative particles (that from now on we will call active particles or A-particles) that bind to nonaggregative particles (NA-particles), as well as to other A-particles. This is done in an agitated tank under transitional (weakly turbulent) flow conditions by means of numerical simulations.

The success of such an aggregation process is expected to depend on the speed of mixing as compared to the speed of aggregation. Mixing is important to disperse the A-particles over the tank volume; if this is not done sufficiently fast, A-particles will attach to nearby other A-particles thereby making them less effective for binding NA-particles. The scenario we explore starts with a fully developed agitated flow of a non-aggregative solid-liquid suspension (all particles in the suspension are NA-particles). At a specific moment in time ($t = 0$) we turn a small fraction of the NA-particles into A-particles and we keep track of the aggregation process that then evolves. In order to identify the role of mixing, we perform the numerical experiments in two ways: (a) the particles turning from NA-particles to A-particles at $t = 0$ are confined to a narrow top layer of the tank, or (b) are randomly distributed over the tank volume. The first situation is akin to A-particles being sprinkled in the tank at the top surface. In the second situation, which is hard to achieve experimentally but easy in a simulation, the A-particles are mixed throughout the tank from the start of the flocculation process.

The simulations that have been performed are of an Eulerian-Lagrangian nature. The volume averaged Navier-Stokes (VANS) equations that govern the liquid flow are solved on a uniform cubic grid (Eulerian) with the lattice-Boltzmann method.[13,14] Individual primary particles are tracked through the flow field (Lagrangian). They move under the influence of hydrodynamic forces, contact forces (including attractive aggregative forces) and gravity. These are particle-unresolved simulations. That is, the Eulerian grid is not sufficiently fine to allow for a direct application of no-slip conditions at particle surfaces and resolve the flow around each particle. This grid spacing is, however, of the same order of magnitude as the particle diameter, a situation we have explored in previous papers.[15,16] Particle motion and fluid motion are two-way coupled: hydrodynamic forces on the particles are fed back to the fluid and the displacement of fluid volume by the particles is accounted for in the VANS equations. While the primary particles move through the mixing tank, the attractive forces the A-particles are equipped with cause aggregation of particles in a fully reversible manner. Aggregates are identified as clusters of primary particles in contact with one another. The simulations allow to assess the size and structure of the aggregates formed as a function of process conditions and particle properties.

The aim of this paper is to explore and quantify, in a computational manner, aggregation processes induced by a relatively small number of active, aggregative particles. The process serves as an example of a strong interrelation between the kinetics of aggregation and multiphase flow dynamics that, we argue, can be effectively described through Eulerian-Lagrangian simulations.

This paper is organized as follows. In the next section, the flow system that has been used will be described in detail and a set of dimensionless numbers characterizing it will be defined. We then summarize the numerical procedure that has been followed and refer to previous papers for further details. Numerical setup and parameters are then given in a subsequent brief section. When discussing results, we focus on visualizing and quantifying the way aggregation and flow are related. A final section summarizes conclusions and provides an outlook to further work.

2 | SOLIDS-LIQUID FLOW SYSTEM

Our mixing tank is cubic with side length T. It has solid walls all around where we apply the no-slip boundary condition. Figure 1 defines the flow configuration and the coordinate system used throughout this paper. Gravity points in the negative z-direction: $\mathbf{g} = -g\mathbf{e}_z$. The impeller revolves around the vertical centre line of the tank and is placed with an off-bottom clearance $C = T/3$. It is a pitched-blade impeller with four 45° inclined blades and has diameter D and revolves with N revolutions per unit time. It pumps the suspension in the negative z-direction. The choice of a cubic tank has been made with a view to (future) validation by quantitative visualization experiments. Undistorted optical access is much helped by planar side, top, and bottom walls.

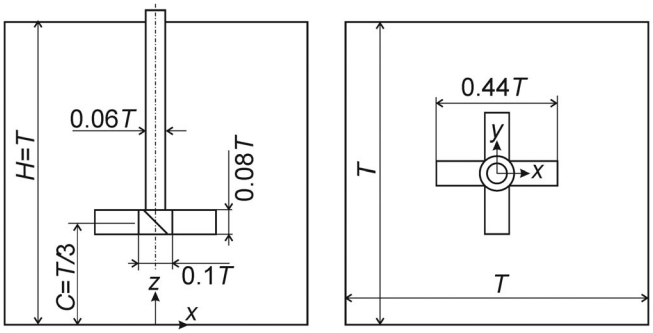

FIGURE 1 Mixing tank geometry: side view (left) and top view (right). The pitched-blade impeller rotates clockwise and thereby pumps liquid in the negative z-direction. The origin of the Cartesian coordinate system is in the centre of the bottom wall. The thickness of the impeller blades is $t_b = 0.021D$

The tank contains a Newtonian liquid with density ρ and kinematic viscosity ν. The solids in the tank are equally sized spheres with diameter d and density $\rho_s > \rho$. As alluded to above, we distinguish between A-particles and NA-particles. A-particles have an attractive interaction with other A-particles as well as with NA-particles. NA-particles have no attractive interaction with other NA-particles. The attractive force, if present, has the same characteristics as in our previous paper.[17] It has two parameters, one (β) defining the strength of interaction, the other (δ_0) the distance over which interaction occurs:

$$\mathbf{F_{ij}} = \beta\frac{\delta_0-\delta}{\delta_0}\frac{(\mathbf{x_j}-\mathbf{x_i})}{|\mathbf{x_j}-\mathbf{x_i}|} \text{ if } 0<\delta<\delta_0, \text{ and } \mathbf{F_{ij}} = \beta\frac{(\mathbf{x_j}-\mathbf{x_i})}{|\mathbf{x_j}-\mathbf{x_i}|} \text{ if } \delta\le 0 \tag{1}$$

where $\mathbf{F_{ij}}$ is the force particle j exerts on particle i (if j and/or i is an A-particle); $\delta = |\mathbf{x_j} - \mathbf{x_i}| - d$ the distance between the two particle surfaces; and $\mathbf{x_i}$ and $\mathbf{x_j}$ their centre locations. From $\delta = \delta_0$ to $\delta = 0$ the magnitude of the (attractive) force increases linearly from 0 to β; if the particles overlap ($\delta < 0$) the force saturates at β. Beyond $\delta = \delta_0$ there is no aggregative force between particle i and j. The total aggregative force experienced by particle i is the sum over particles j within the $\delta_0$vicinity of i: $\mathbf{F_i} = \sum_{j\neq i}\mathbf{F_{ij}}$. In addition to aggregative forces, particles also interact through lubrication forces, as well as through soft-sphere repulsive interaction forces. These will be discussed in the next section.

Our flow system has been defined in terms of a set of dimensionless numbers. The impeller-based Reynolds number $\mathrm{Re} = ND^2/\nu$ characterizes the overall flow conditions in the tank. A Shields number $\theta = \frac{\rho N^2 D^2}{gd(\rho_s-\rho)}$ reflects the competition between inertial liquid stresses (proportional to $\rho N^2 D^2$) suspending particles and net gravity pulling them down. The overall solids volume fraction is $\langle\phi\rangle = n\frac{\pi}{6}d^3/T^3$, where n is the total number of particles (A-particles plus NA-particles) in the tank. The density ratio ρ_s/ρ quantifies the inertia of the solids relative to the liquid. The interaction distance of the aggregation force has been nondimensionalized by the diameter of the particles: $\delta_a = \delta_0/d$. The strength of the aggregation force has been scaled with the weight of a particle: $\beta_a = \beta/g\rho_s\frac{\pi}{6}d^3$. Finally, the symbol f is used for the fraction of A-particles, that is, the number of A-particles divided by the total number of particles in the tank.

TABLE 1 List of dimensionless numbers and their values/ranges

D/T	**0.436**
C/T	0.333
$\mathrm{Re} = ND^2/\nu$	4000
$\langle\phi\rangle = n\frac{\pi}{6}d^3/T^3$	0.0983
$f = n_{ac}/n$	0.058
ρ_s/ρ	2.23
$\beta_a = \beta/g\rho_s\frac{\pi}{6}d^3$	1-9
$\delta_a = \delta_0/d$	0.40
$\theta = \rho N^2D^2/gd(\rho_s-\rho)$	260

Table 1 lists the values of the dimensionless numbers. The major variable in this study is the aggregation strength β_a that was in the range 1-9. In previous work,[17] it was shown that the distance of aggregative interaction had limited effect on the levels of aggregation and on the overall flow behaviour of the solids-liquid suspension. For that reason, we gave δ_a a fixed value.

3 | NUMERICAL PROCEDURES

The equations to be solved, the numerical procedures, as well as the models that are used for the solids-liquid flow dynamics are similar to those in other work.[15,16] The additional feature of an aggregative force has been discussed in Lim and Derksen.[17] At the core of the simulation process is solving the volume-averaged continuity and volume-averaged Navier-Stokes equations[18]:

$$\frac{\partial}{\partial t}(\rho\phi^c) + \nabla\cdot(\rho\phi^c\mathbf{u}) = 0 \tag{2}$$

$$\frac{\partial}{\partial t}(\rho\phi^c\mathbf{u}) + \nabla\cdot(\rho\phi^c\mathbf{uu}) = \phi^c\nabla\cdot\boldsymbol{\pi} + \mathbf{f_s} \tag{3}$$

where $\phi^c \equiv 1-\phi$ is the liquid phase volume fraction and ϕ the solids volume fraction; $\mathbf{u}$ the interstitial liquid

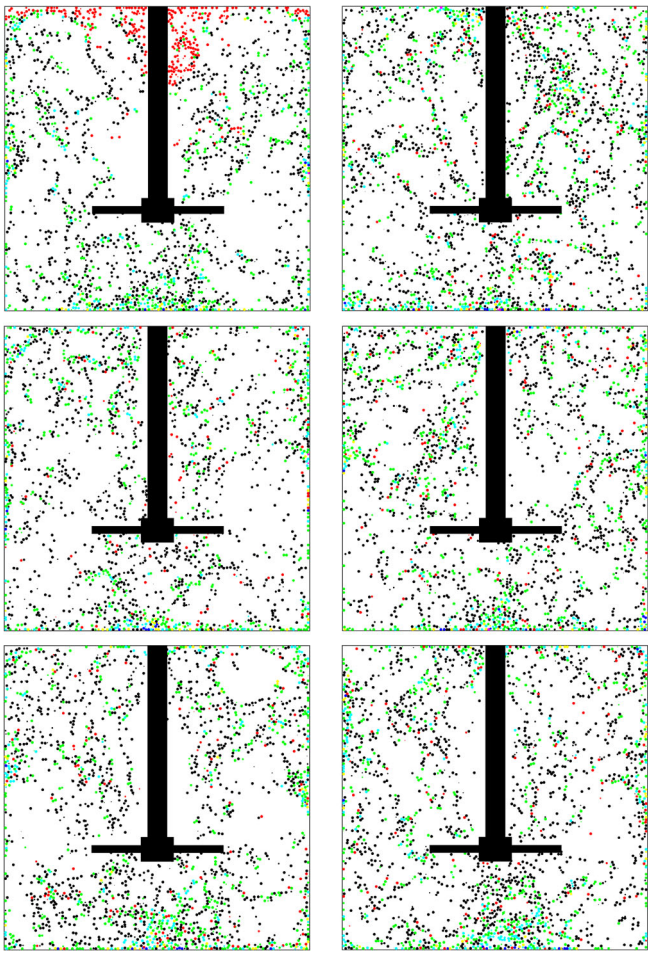

FIGURE 2 Snapshot of particles in yz slice with thickness d through the centre of the tank for the *TA* system (left) and *RDA* system (right), both with $\beta_a = 1$ and $\delta_a = 0.4$: $tN = 2$, 10, 50 (top to bottom). Colour coding: red: active particles; black: single particle; green: a doublet; cyan: a triplet; yellow: a quartet; blue: a quintet; magenta: an aggregate of six or more particles

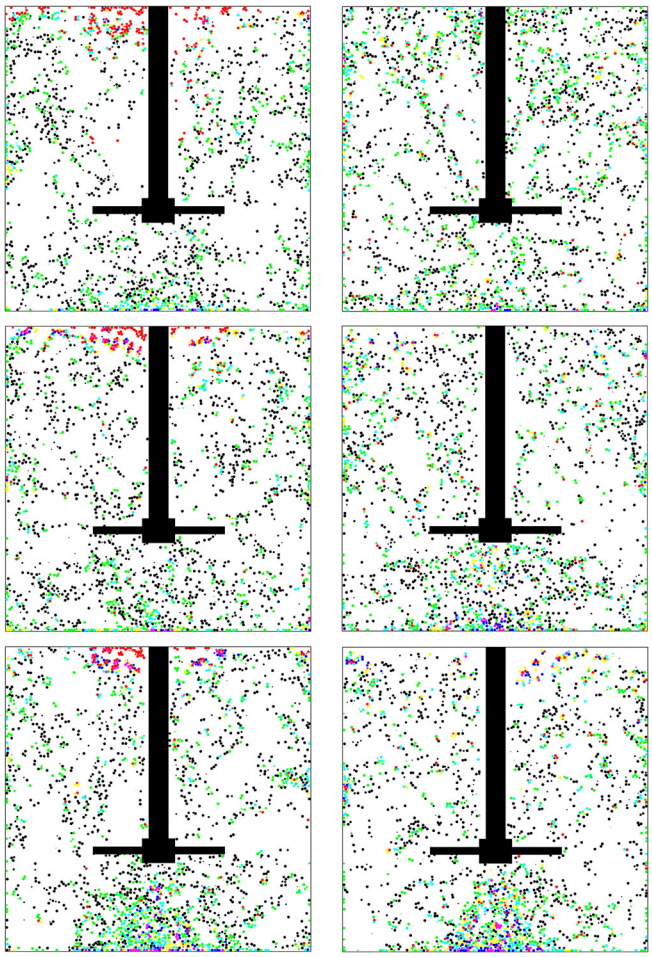

FIGURE 3 Snapshot of particles in yz slice with thickness d through the centre of the tank for the *TA* system (left) and *RDA* system (right), both with $\beta_a = 9$ and $\delta_a = 0.4$: $tN = 2$, 10, 50 (top to bottom). Colour coding: red: active particles; black: single particle; green: a doublet; cyan: a triplet; yellow: a quartet; blue: a quintet; magenta: an aggregate of six or more particles

velocity; $\boldsymbol{\pi}$ the liquid's stress tensor (that obeys Newtonian rheology); and $\mathbf{f_s}$ the force per unit volume the solid particles exert on the liquid. The fluid flow thus feels the presence of particles through the volume displaced by the particles (the ϕ^c terms in Equations (1) and (2)) as well as through the solids-liquid interaction force $\mathbf{f_s}$. Solving this set of equations is done numerically by means of an extended lattice-Boltzmann method on a uniform, cubic, three-dimensional grid with grid spacing Δ.[19] Time advances in a discrete manner with a time step Δt.

The solids volume fraction in each grid cell is acquired from the location of the particles. Assigning solid volume to a grid cell involves a mapping process,[15,20] where, in three dimensions, clipped fourth-order polynomials centred around the centre location of a particle are used as a weighing function to distribute solids volume over grid cells in the direct vicinity of the particle.[21] As previously,[15] we have set the mapping function's half-width to $\lambda = 1.5d$. An important attribute of this mapping process is that it allows the particle size to be of the same order as the grid spacing, $d = O(\Delta)$.[15] As a result, we can choose the grid spacing independent of the particle size. This is important in cases where the choice of grid spacing is dictated by the (turbulent) characteristics of the liquid flow and not directly by the particle size.[16]

Where above mapping has been used to assign Lagrangian information (particle locations) to the solids volume fraction distribution over the (Eulerian) grid, mapping has also been used to transfer Eulerian properties to Lagrangian properties. For determining the drag force $\mathbf{F_D}$ on each particle we need the fluid velocity $\mathbf{u_f}$ in the direct vicinity of the particle. This we map from the Eulerian velocity field on the grid ($\mathbf{u}$) to the location of

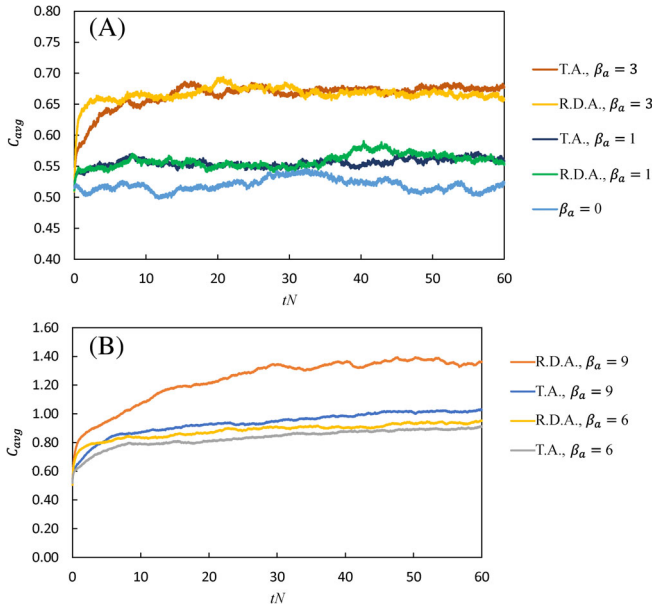

FIGURE 4 Average coordination number C_{avg} as a function of time for nonaggregating, *TA* system and *RDA* system with $\delta_a = 0.4$: A, $\beta_a = 0, 1, 3$; B, $\beta_a = 6, 9$

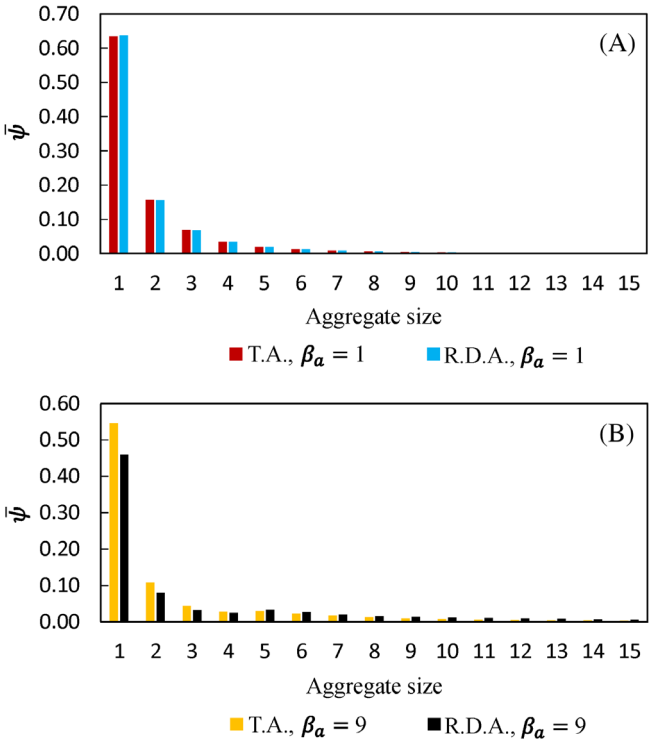

FIGURE 5 Aggregate size distributions averaged over the time-interval $40 \leq tN \leq 60$ for *TA* system and *RDA* system: A, $\beta_a = 1$; and B, $\beta_a = 9$. The symbol ψ indicates the volume of solids contained in each size class divided by the total volume of solids

the particle with the same mapping functions as used above.

The drag force is written as follows:

$$\mathbf{F_D} = 3\pi\rho v d\left(\mathbf{u_f} - \mathbf{u_p}\right) F\left(\mathrm{Re}_p, \phi\right) \tag{4}$$

where $\mathrm{Re}_p = (1-\phi)|\mathbf{u_f} - \mathbf{u_p}|d/v$ is the particle-based Reynolds number; and $\mathbf{u_p}$ the particle velocity. The function F, that represents the way drag depends on the Reynolds number and the (local) solids volume fraction, has been decomposed as $F(\mathrm{Re}_p, \phi) = p(\mathrm{Re}_p)q(\phi)$, with $p\left(\mathrm{Re}_p\right) = \left(1 + 0.15\mathrm{Re}_p^{0.687}\right)$ the Schiller-Naumann correction to Stokes drag[22] and $q(\phi) = (1-\phi)^{-2.65}$ the Wen and Yu correlation.[23] Wen and Yu drag was demonstrated to be suitable for solid-liquid systems that have moderate Stokes numbers.[24] The drag force is fed back, again through mapping, to the liquid as the hydrodynamic force per unit volume exerted by the particles on the liquid $\mathbf{f_s}$, see Equation (3).

The translational equation of motion for a particle reads as follows:

$$m_p \frac{d\mathbf{u}_\mathrm{p}}{dt} = \mathbf{F_H} + \mathbf{F_C} + \mathbf{F_L} + \mathbf{F_A} - \frac{\pi}{6} d^3 (\rho_s - \rho)\mathrm{g}\mathbf{e_z} \tag{5}$$

$$\frac{d\mathbf{x}_\mathbf{p}}{dt} = \mathbf{u_p} \tag{6}$$

where $m_p = \rho_s \frac{\pi}{6} d^3$ is the mass of a particle. The forces felt by the particle are the hydrodynamic force $\mathbf{F_H} = \mathbf{F_D}/\phi$,[25] a soft-sphere linear elastic collision force $\mathbf{F_C}$, a lubrication force $\mathbf{F_L}$, an aggregation force $\mathbf{F_A}$, and net gravity. The way the aggregation force is calculated was discussed in the previous section. Both contact and lubrication force are assumed to be radial forces, that is, they act on a line connecting the centres of two interacting particles. For the collision force this implies smooth particles with zero friction. For the lubrication force it means that we only consider radial lubrication and discard tangential lubrication which, in general, is much weaker than radial lubrication: radial lubrication is inversely proportional to the distance between particle surfaces, tangential lubrication with the logarithm of that distance. Detailed expressions for $\mathbf{F_C}$ and $\mathbf{F_L}$ are given in Derksen.[15] Equation (6) is solved for each individual primary particle with an explicit discretization of the acceleration term through mixed time derivatives[26]; mixed derivatives enhance stability. The time step used is the same Δt as used to advance the LBM for the liquid flow. We only solve the translational equations of motion of the particles, not the rotational ones. This is justified by the fact that we consider smooth collisions that do not generate angular momentum as well as the weak back-effect spherical particle rotation would have on the liquid flow.

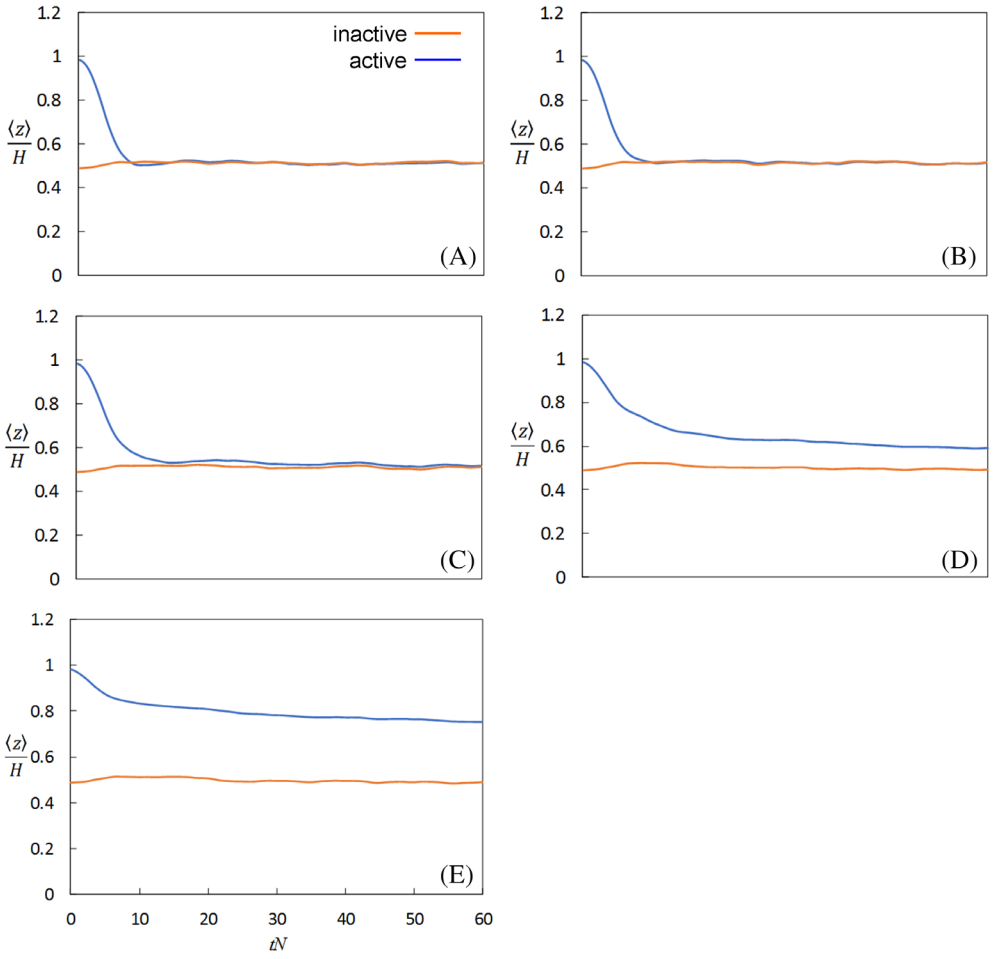

FIGURE 6 Averaged location of active and inactive particles in z-direction for: A, $\beta_a = 0$; and TA system: B, $\beta_a = 1$; C, $\beta_a = 3$; D, $\beta_a = 6$; and E, $\beta_a = 9$

The no-slip boundary conditions for the liquid flow at the bounding planar walls of the cubic mixing tank have been imposed by applying the halfway bounce-back rule to the LB distribution functions.[14] An immersed boundary method has been used to impose no-slip at the revolving impeller.[27] The collisions between particles and solid walls (outer walls and impeller surface) use the same linear elastic force as used for particle-particle collisions.

4 | SET-UP OF SIMULATIONS

The spatial resolution with which we solve the liquid flow is such that the side length of the tank spans 110 lattice spacings: $T = 110\Delta$ and the impeller diameter $D = 48\Delta$. One impeller revolution is completed in 1600 time steps: $N = (1600\Delta t)^{-1}$. With these settings the impeller tip speed is $v_{tip} = \pi ND = 0.094\Delta/\Delta t$. The tip speed is a good measure for the highest liquid velocities in the tank. Then the tip speed being an order of magnitude lower than $\Delta/\Delta t$ implies we are solving nearly incompressible flow with the (compressible) LBM [14]. In order to achieve an impeller-based Reynolds number of 4000, the viscosity was set to $\nu = 3.6 \cdot 10^{-4}\Delta^2/\Delta t$. This modest Reynolds number was chosen to create mildly turbulent, or at least transitional, flow while not needing a subgrid-scale model. This way we avoid such questions as how to deal with particle motion as a result of unresolved fluid flow fluctuations.

The particle diameter has been set to $d = \Delta = D/48$. With $n = 250,000$ particles we reach a tank-averaged solids volume fraction of $\langle\phi\rangle = 0.0983$. The number of active particles is $n_A = 14,584$ so that $f = n_A/n = 0.058$. With the density ratio set to $\rho_s/\rho = 2.23$ (eg, quartz sand in water) we set gravitational acceleration to $g = 3.06 \cdot 10^{-6}\Delta/\Delta t^2$ in order to have a Shields number of $\theta = 260$.

Previous work[17] has shown that the reach of the attractive force δ_a is not a critical parameter for the levels of aggregation reached. It has a fixed value of $\delta_a = 0.4$ in this paper. The strength of the aggregative force β_a is decisive for the aggregative process[17]; it is the main independent variable in this paper and has been varied in the range 1-9.

The starting point of the simulations in this paper is a fully developed system of nonaggregative particles. Given

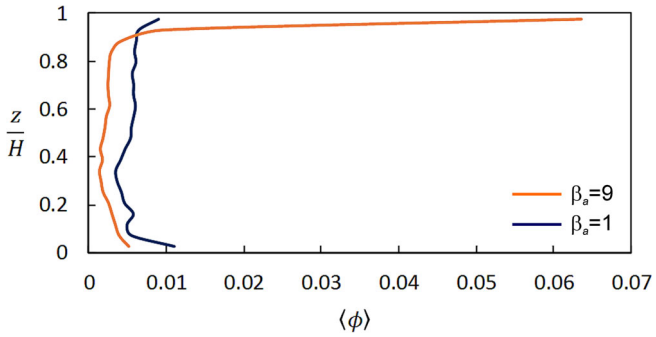

FIGURE 7 Time-averaged (over $40 \leq tN \leq 60$) solids volume fraction of active particles as a function of z for *TA* systems with $\beta_a = 1$ and $\beta_a = 9$

its Shields number of $\theta = 260$, this is a fully suspended system (no particles resting on the bottom) that, however, does show particle concentration gradients.[17] Then, at time equal zero ($t = 0$) a fraction f of the total number of particles is turned into A-particles according to two different scenarios. Scenario TA (top A-particles): all A-particles are confined to the top of the tank in a layer with thickness $4d$. Scenario RDA (randomly distributed A-particles): A-particles are randomly distributed over the tank volume.

5 | RESULTS

Qualitative impressions showing some of the main features of particle behaviour, aggregation, and its time scales are given in Figures 2 and 3. The panels in each figure show instantaneous realizations of particles in a vertical cross section through the centre of the tank. In Figure 2 we show a weakly aggregative system ($\beta_a = 1$), in Figure 3 a strongly aggregative system ($\beta_a = 9$). In each figure we compare the *TA* scenario on the left side with the *RDA* scenario on the right side. The top panels of Figure 2 (that are at $tN = 2$) clearly show the difference in the way the active particles have been initialized. At that moment of the aggregation process, most of the red (is A) particles are still in the top part of the tank if they were initialized there. In the later stages shown in Figure 2, that is, $tN = 10$ and $tN = 50$, there is no obvious difference between the *TA* and the *RDA* scenario. This is much different for Figure 3. There the most striking difference between *TA* and *RDA* is that for *TA* a large part of the A-particles persistently remains in the top region of the tank where they have aggregated. We also see that levels of aggregation in the *RDA* scenario are higher than in the *TA* scenario after 50 impeller revolutions. Both scenarios show significant accumulations of solids underneath the impeller.

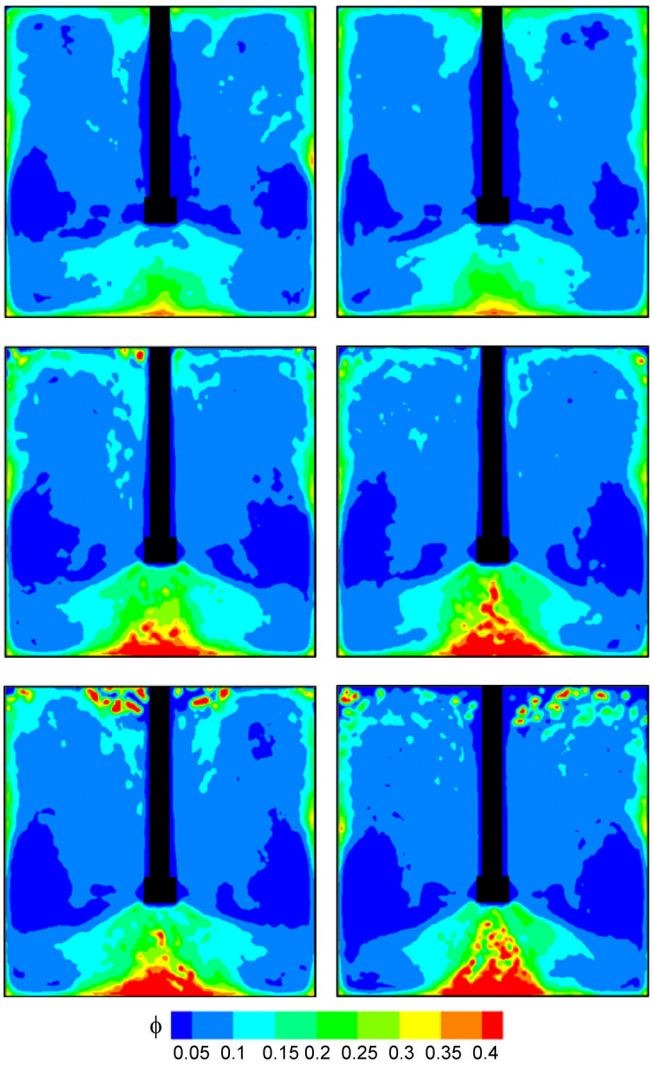

FIGURE 8 Time-averaged solids volume fraction contours over 20 impeller revolutions ($40 \leq tN \leq 60$) for *TA* system (left) and *RDA* system (right) in a vertical plane through the centre of the mixing tank for different aggregation strength $\beta_a = 1, 6, 9$ (top to bottom)

One quantitative measure of aggregation is the tank-averaged coordination number, which is the average number of other particles a particle is in contact with, where contact is defined as touching or overlapping of particles; $\delta \leq 0$ in the terminology of Equation (1). The way the tank-averaged coordination number evolves in time is shown in Figure 4. As a baseline, we include in this figure a time series for a system without any aggregative particles (the line $\beta_a = 0$ in Figure 4A). We see that if $\beta_a = 1$, *TA* as well as *RDA* systems are only marginally aggregating with C_{avg} hardly rising above the noise compared to the baseline. The data for $\beta_a = 3$ (in Figure 4A) hint at some interesting features: at this strength of the aggregative force the systems are clearly aggregating. The

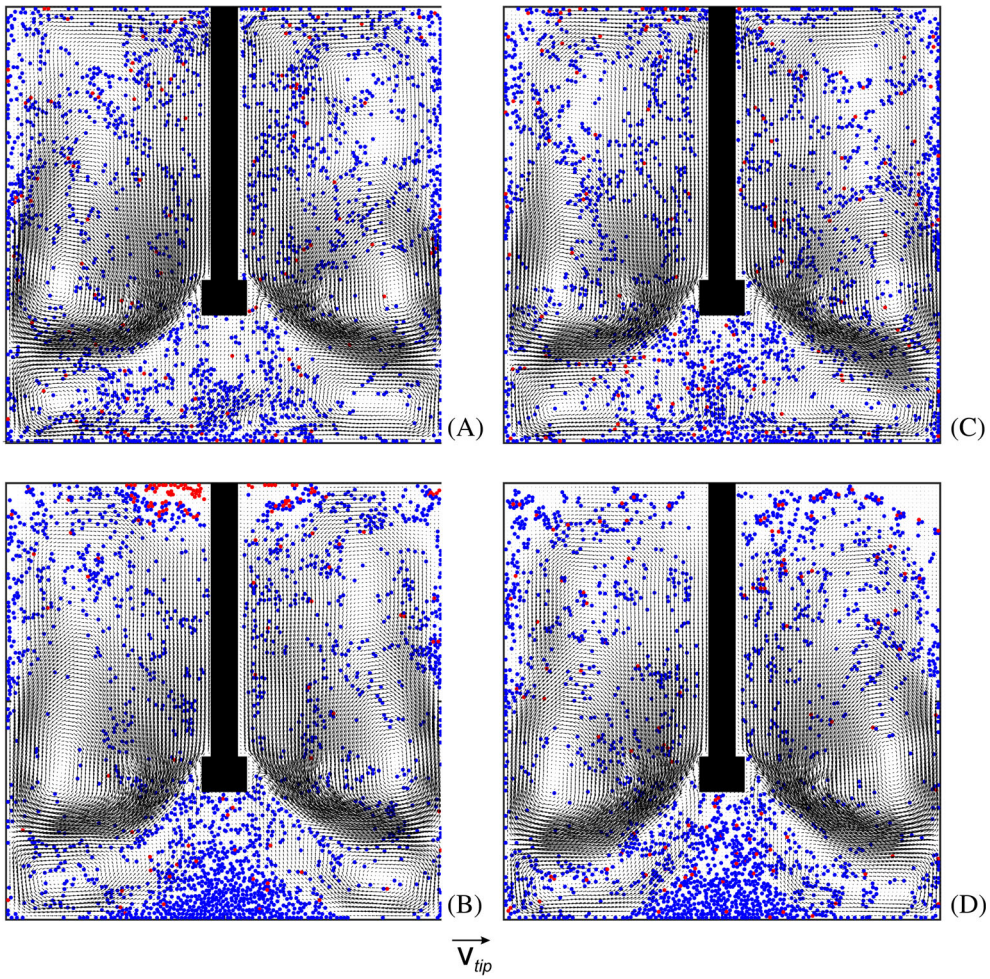

FIGURE 9 Time-averaged (over $40 \leq tN \leq 60$) liquid velocity vectors in a yz plane and the snapshot of particles through the centre of the tank at $tN = 60$ for *TA* system with: A, $\beta_a = 1$; and B, $\beta_a = 9$ and *RDA* system with: C, $\beta_a = 1$; and D, $\beta_a = 9$. Colour coding: red active particles and blue inactive particles

eventual state of aggregation does not differ between *TA* and *RDA*. The speed of aggregation is, however, significantly faster for the *RDA* system. Where it takes ~1.4 impeller revolutions for the *RDA* system to reach 90% of its eventual steady C_{avg} value, the *TA* system requires 4.7 impeller revolutions for this. Here we clearly observe the interaction of mixing and aggregation. Where the *TA* system needs time to spread (mix) the A-particles over the tank volume, the already mixed *RDA* system is from the beginning up to speed when it comes to aggregation. The fact that the steady state C_{avg} values agree between the *TA* and *RDA* scenario is an indication that the flow in the tank is able to sufficiently distribute the A-particles possessing $\beta_a = 3$ over the volume.

In Figure 4B, the strength of the aggregative force is increased further (where we must note the difference in the scale of the vertical axis as compared to 4A). The $\beta_a = 6$ time series of C_{avg} show similar trends as the ones for $\beta_a = 3$, although now the steady-state C_{avg} for *RDA* is slightly but consistently above its *TA* counterpart. For $\beta_a = 9$, the latter effect is strongly amplified: aggregation in the *RDA* scenario clearly outperforms that in the *TA* scenario. This suggests a situation where the activity of the A-particles gets reduced because they aggregate among one another before they have had the opportunity to spread through the tank volume. This was anticipated when discussing Figure 3, specifically its lower left panel. It shows A-particles preferentially staying in the top part of the tank, even after 50 impeller revolutions.

The aggregate size distributions given in Figure 5 confirm the observations on solids mixing and aggregation made so far. For $\beta_a = 1$ there is no significant difference between *TA* and *RDA* scenarios. For $\beta_a = 9$ the *TA* system has aggregated less than the *RDA* system with a significantly larger number of single particles for *TA* and significantly higher numbers of larger aggregates ($n_a \geq 5$) for *RDA*.

Given that in the *TA* systems the A-particles and NA-particles are initially segregated vertically with the A-particles occupying the top layer with thickness $4d$ of the tank, an effective way to quantify solids mixing is by monitoring the average vertical location $\langle z \rangle$ of the two particle types separately. We do so in Figure 6. This gives further insight in the way aggregation and mixing interact. In the *TA* scenario solids mixing is clearly achieved if $\beta_a \leq 3$: In steady state the average z-location of A-

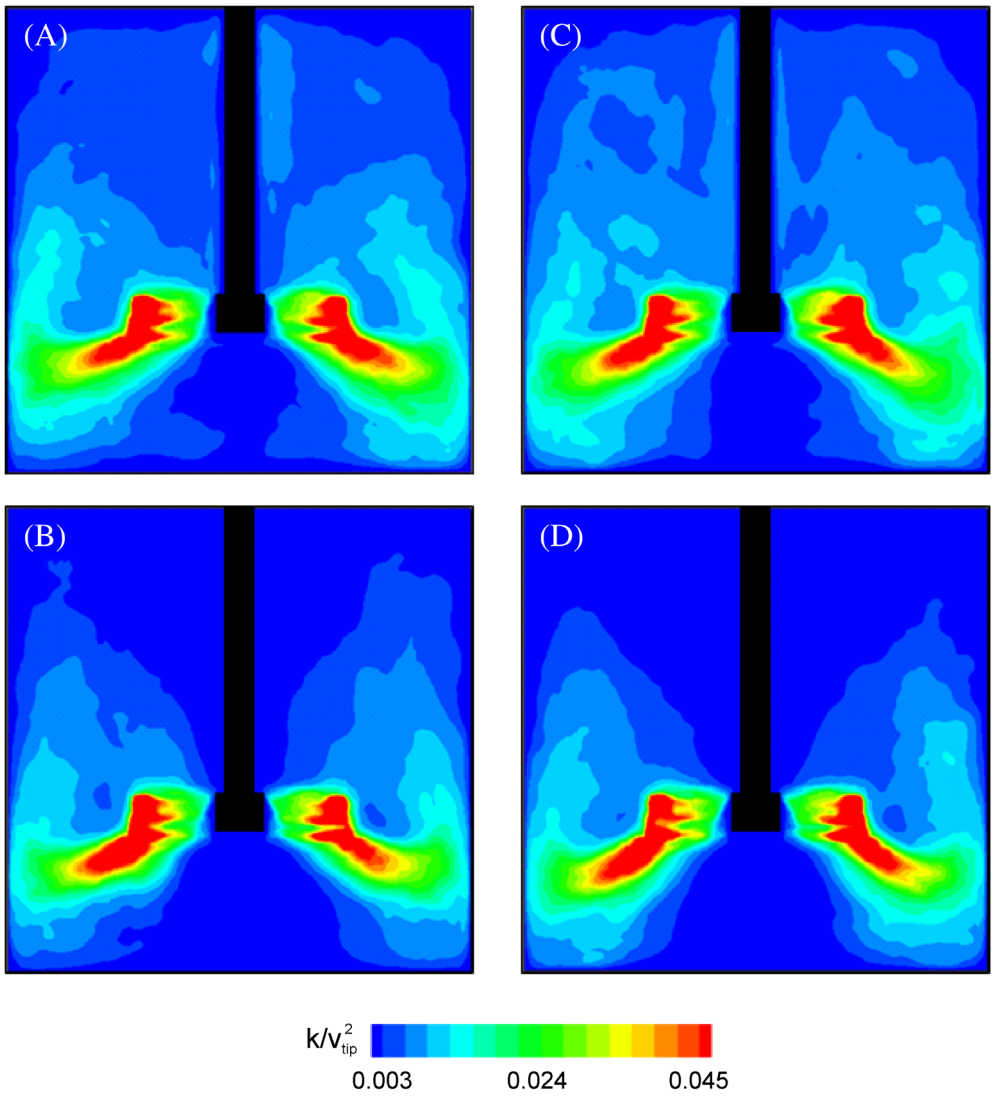

FIGURE 10 Time-averaged turbulent kinetic energy (normalized by the square of the impeller tip speed, v_{tip}^2) in the vertical *yz* plane through the centre of the tank. Averaging over 20 impeller revolutions, $40 \leq tN \leq 60$ for *TA* system with: A, $\beta_a = 1$; and B, $\beta_a = 9$; *RDA* system with: C, $\beta_a = 1$; and D, $\beta_a = 9$

particles and NA-particles is the same and close to $0.5H$. If, for these cases, we quantify the mixing time by the moment $\langle z \rangle / H$ of A-particles and NA-particles is within 0.01, a slight increase of the mixing time is observed if $\beta_a = 3$ as compared to $\beta_a = 1$ and $\beta_a = 0$. For $\beta_a \geq 6$ proper solids mixing of the A-particles is not achieved with, as we saw earlier, negative consequences for the levels of aggregation.

Figure 7 reiterates how the aggregation strength influences solids mixing. Vertical profiles of the time-averaged volume fraction of A-particles are shown for *TA* systems. Over the time averaging window ($40 \leq tN \leq 60$) the systems are dynamically steady. For the strongly aggregating system, the A-particles do not mix well. They preferentially stay in the top region of the tank and are there not effective for aggregating the NA-particles.

In general, aggregation has impact on the distribution of solids throughout the tank.[17] For the systems we have been dealing with, this is illustrated in Figure 8. We show the time-averaged solids volume fraction distribution in a vertical cross section in the mixing tank for six of the systems we have been simulating. From top to bottom the aggregative strength β_a is increased. The left column shows *TA* scenarios; the right column *RDA* scenarios. The most significant effect is the formation of a solids cone underneath the impeller and resting on the bottom of the tank for an aggregation strength of $\beta_a \geq 6$. This means that the aggregation process "works". The aggregative particles are able to settle out a significant part of the solids present in the tank. The difference between $\beta_a = 6$ and $\beta_a = 9$ in terms of the solids cone is marginal; it is much weaker than the effect of the initialization of the A-particles. The more effective aggregation in the *RDA* scenario brings much more solids to the bottom region of the mixing tank.

The way the liquid flow feels the levels of aggregation is the subject of Figures 9 (average flow) and 10 (turbulent kinetic energy). In all cases, the overall flow pattern

shows a strong, inclined downward jet coming off the impeller. The increased particle concentrations near the bottom when $\beta_a = 9$ make a weaker flow in the region directly above the bottom as compared to $\beta_a = 1$. It is interesting to see in Figure 9 that for $\beta_a = 9$ in the *RDA* scenario the A-particles form the core of a number of aggregates that, at this moment in time ($tN = 60$), are still in the region above the impeller. Turbulent kinetic energy is very inhomogeneously distributed in the mixing tank with the impeller-swept volume and the impeller outstream being hot spots (Figure 10). The, minor, differences in the panels of Figure 10 relate to the very bottom region. With the weaker aggregative force of $\beta_a = 1$, turbulence coming from the impeller reaches closer to the bottom compared to $\beta_a = 9$ because in the latter case the solids concentrations are much higher there.

6 | CONCLUSIONS

This paper focuses on the interaction between solids mixing and aggregation in a computational manner. For this an Eulerian-Lagrangian simulation method that allows for a choice of the (Eulerian) grid spacing independent of particle size has been used. We explore scenarios where we release a relatively small number of active, aggregative particles in a mixing tank in order to bind a much larger number of non-aggregative particles. We demonstrate that spreading the active particles through the mixing tank is a crucial step in the aggregation process. We do this by comparing a premixed scenario with a scenario that, initially, has the active particles segregated from the rest of the particles. The premixed case is a fictitious reference case that can only be realized in a simulation, not in a practical (real) flow configuration. The segregated case has the potential of being mimicked in an experiment.

For active particles equipped with relatively weak aggregation forces, aggregation time scales are long relative to the time scales of mixing. This allows the active particles to spread through the tank volume before they bind to one another. In these situations, there is hardly any difference in the eventual aggregation performance, for example, measured by means of the volume-average coordination number, between premixed and segregated initial conditions. Only the time to reach steady-state aggregation levels is somewhat longer for the segregated initial condition. The stronger the relative aggregation force β_a, the shorter it takes for active particles to bind to another. This has significant consequences for overall aggregation since now the active particles are unable to spread through the tank and by binding to one another become less effective for also binding inactive particles.

The levels of aggregation are found to have impact on the distribution of solids through the mixing tank. High levels of aggregation lead to the formation of a solids cone on the bottom of the tank, underneath the impeller which is an indication of the success of the aggregation process if its purpose is to separate solids and liquid. The formation of the solids cone has some minor effects on the average flow patterns in the tank as well as on the spatial distribution of turbulent kinetic energy.

REFERENCES

[1] H. Wang, M. Lin, D. Chen, Z. Dong, J. Zhang, *Powder Technol.* **2018**, *331*, 310.
[2] H. Mumtaz, M. Hounslow, N. Seaton, W. Paterson, *Chem. Eng. Res. Des.* **1997**, *75*, 152.
[3] J. Kim, T. A. Kramer, *Chem. Eng. Sci.* **2006**, *61*, 45.
[4] M. Bäbler, M. Morbidelli, J. Baldyga, *J. Fluid Mech.* **2008**, *612*, 261.
[5] M. Breuer, A. Khalifa, *Powder Technol.* **2019**, *348*, 105.
[6] M. Von Smoluchowski, *Z. Phys. Chem.* **1917**, *92*, 129.
[7] E. D. Hollander, J. J. Derksen, L. M. Portela, H. E. A. van den Akker, *AIChE J.* **2001**, *47*, 2425.
[8] D. Ramkrishna, *Population Balances*, Academic Press, London **2000**.
[9] P. Bubakova, M. Pivokonsky, P. Filip, *Powder Technol.* **2013**, *235*, 540.
[10] J. Morchain, J.-C. Gabelle, A. Cockx, *AIChE J.* **2014**, *60*, 27.
[11] K. Hayashi, S. Watano, *Powder Technol.* **2019**, *342*, 664.
[12] J. T. G. Overbeek, *Powder Technol.* **1984**, *37*, 195.
[13] S. Chen, G. D. Doolen, *Annu. Rev. Fluid Mech.* **1998**, *30*, 329.
[14] S. Succi, *The Lattice Boltzmann Equation for Fluid Dynamics and Beyond*, Clarendon Press, Oxford **2001**.
[15] J. J. Derksen, *Comput. Fluids* **2018**, *176*, 266.
[16] J. J. Derksen, *AIChE J.* **2018**, *64*, 1147.
[17] J. W. Lim, J. J. Derksen, *Chem. Eng. Res. Des.* **2019**, *152*, 278.
[18] K. Sankaranarayanan, S. Sundaresan, *Ind. Eng. Chem. Res.* **2008**, *47*, 9165.
[19] R. Sungkorn, J. J. Derksen, *Phys. Fluids* **2012**, *24*, 123303.
[20] J. Capecelatro, O. Desjardins, *J. Comput. Phys.* **2013**, *238*, 1.
[21] N. G. Deen, M. V. S. Annaland, J. A. M. Kuipers, *Chem. Eng. Sci.* **2004**, *59*, 1853.
[22] L. Schiller, A. Naumann, *Ver. Deut. Ing. Z.* **1933**, *77*, 318.
[23] C. Y. Wen, Y. H. Yu, *Chem. Eng. Prog.* **1966**, *62*, 100.
[24] G. J. Rubinstein, J. J. Derksen, S. Sundaresan, *J. Fluid Mech.* **2016**, *788*, 576.
[25] J. J. Derksen, S. Sundaresan, *J. Fluid Mech.* **2007**, *587*, 303.
[26] Z. G. Feng, E. Michaelides, *Comput. Fluids* **2009**, *38*, 370.
[27] J. Derksen, H. E. A. Van den Akker, *AIChE J.* **1999**, *45*, 209.

How to cite this article: Lim JW, Derksen JJ. Adding active particles for overall aggregation in a mixing tank: A computational study. *Can J Chem Eng*. 2020;98:2451–2460. https://doi.org/10.1002/cjce.23764